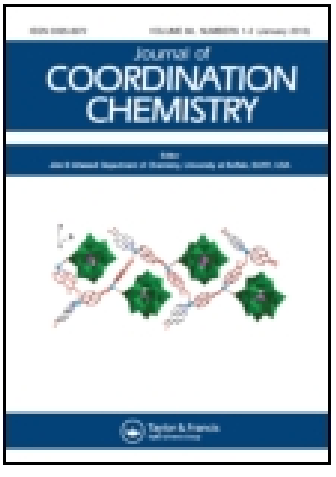

Journal of Coordination Chemistry
Publication details, including instructions for authors and subscription information:
http://www.tandfonline.com/loi/gcoo20

Synthesis, crystal structure, magnetism, and biological activities of an oxo-bridged diiron(III) complex

Bi-Wei Wang[abc], Lin Jiang[abc], Zhang Dong[abc], Bo-Wen Li[abc], Si-Sheng Shu[abc], Wen Gu[abc], Xin Liu[abc] & Jin-Lei Tian[abc]

[a] Department of Chemistry, Nankai University, Tianjin, PR China

[b] Tianjin Key Laboratory of Metal and Molecule Based Material Chemistry, Tianjin, PR China

[c] Key Laboratory of Advanced Energy Materials Chemistry (MOE), Tianjin, PR China

Accepted author version posted online: 05 Jun 2014.Published online: 02 Jul 2014.

To cite this article: Bi-Wei Wang, Lin Jiang, Zhang Dong, Bo-Wen Li, Si-Sheng Shu, Wen Gu, Xin Liu & Jin-Lei Tian (2014) Synthesis, crystal structure, magnetism, and biological activities of an oxo-bridged diiron(III) complex, Journal of Coordination Chemistry, 67:12, 2062-2075, DOI: 10.1080/00958972.2014.931574

To link to this article: http://dx.doi.org/10.1080/00958972.2014.931574

Journal of Coordination Chemistry, 2014
Vol. 67, No. 12, 2062–2075, http://dx.doi.org/10.1080/00958972.2014.931574

Synthesis, crystal structure, magnetism, and biological activities of an oxo-bridged diiron(III) complex

BI-WEI WANG†‡§, LIN JIANG†‡§, ZHANG DONG†‡§, BO-WEN LI†‡§, SI-SHENG SHU†‡§, WEN GU†‡§, XIN LIU†‡§ and JIN-LEI TIAN*†‡§

†Department of Chemistry, Nankai University, Tianjin, PR China
‡Tianjin Key Laboratory of Metal and Molecule Based Material Chemistry, Tianjin, PR China
§Key Laboratory of Advanced Energy Materials Chemistry (MOE), Tianjin, PR China

(*Received 29 December 2013; accepted 1 May 2014*)

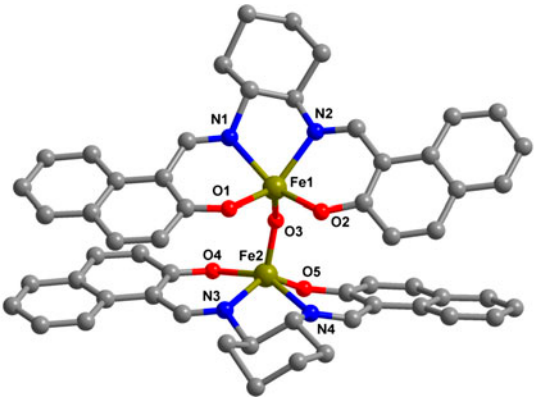

An unsymmetrical oxo-bridged diiron(III) complex has been synthesized and its biological activities have been characterized by various physico-chemical techniques.

An unsymmetrical oxo-bridged diiron(III) complex $[Fe_2\mathbf{L}_2(\mu\text{-O})]$, {$H_2\mathbf{L}$ = trans-N,N′-bis-(2hydroxy-1-naphthalidehydene)-cyclohexanediamine} has been synthesized and characterized by various physico-chemical techniques. In the complex, each deprotonated bi-anionic $\mathbf{L}^{2-}$ serves as a terminal tetradentate ligand (N_2O_2) and coordinates to one Fe to form a $[Fe\mathbf{L}]^+$ unit. Two $[Fe\mathbf{L}]^+$ units are further linked by an oxo-bridge to construct the binuclear oxo-Fe species with intramolecular Fe–Fe separation of 3.38 Å. Variable-temperature magnetic susceptibility studies revealed a strong antiferromagnetic interaction between two iron centers with J of $-112\ cm^{-1}$. The interaction of the complex with CT-DNA was studied by various spectroscopic and viscosity measurements, which indicated that the complex could interact with CT-DNA through intercalation. In addition, the complex is able to cleave pBR322 DNA in the presence of H_2O_2. Furthermore, the interaction of the compound with BSA was also investigated, which indicated that the complex could quench the intrinsic fluorescence of BSA by a static quenching mechanism.

Keywords: Oxo-bridged binuclear iron; Schiff base ligand; Magnetic property; DNA binding

*Corresponding author. Email: tiant@nankai.edu.cn

1. Introduction

The reaction of the fracture and recombinant on nucleic acids is a core technology in the field of molecular biology and genetic engineering, which mainly focuses on a localization fracture of DNA and RNA [1, 2]. Over the last decade, increasing attention has been gained by the development of synthetic hydrolases (e.g. artificial nucleases), which produce many types of macromolecules *in vivo* such as phospholipids, proteins, and nucleic acids through catalyzed hydrolytic cleavage [3–5]. As highlighted by several reviews [6–8], numerous significant theoretical and practical features have been discovered for artificial cleavage agents, for instance: (1) for easier access to the steric region of DNA due to its small size, which allows the continued advancement of catalytic mechanism of nuclease; (2) for the treatment of tumors and genetic diseases as chemotherapy drugs (e.g. cisplatin [9] and second-generation alternatives carboplatin and oxaliplatin [10]); (3) as a probe of secondary and tertiary structure of nucleic acids; and (4) as tools for genetic isolate, genetic sequence analysis, and DNA mutagenesis [11]. Compared with natural nucleases that possess metal ions in their active sites, several categories of artificial nucleases have been designed using metal-based complexes.

Due to the development of new therapeutic agents and novel nucleic acid structural probes, interest in development of Schiff bases has attracted much attention [12–15]. As a previous study demonstrated [16], the azomethine linkage in the structure could be responsible for biological activities including antitumor, antibacterial, antifungal, and herbicidal activity. The preparative accessibility, structural variety, and capability to stabilize different metals in various oxidation states have led to Schiff base ligands being considered as a 'privileged ligand' [17]. In comparison to the free ligand, anticancer activity as metal complexes has been enhanced [18]. Thus, various metal ions have been employed in combination with Schiff base ligands, including some lanthanides (Ho^{3+}, Eu^{3+}, La^{3+}, Dy^{3+}, Yb^{3+}) [19–23], as well as several first-row transition metal ions (Cu^{2+}, Ni^{2+}, Co^{2+}, Zn^{2+}, Cr^{3+}) [24, 25]. Transition metal complexes as synthetic metallonucleases have been studied extensively due to their supporting a multitude of coordination numbers and geometries. Among them, iron compounds result in the most active synthetic nucleases due to higher oxidation states and stronger Lewis acidity. Ferric complexes are involved in transition states of many organism reactions [26–29], but they have been scarcely employed for artificial nucleases different from Fe(II) and Zn(II).

Due to coplanar aromatic rings, naphthalene is regarded as an efficient DNA intercalating group. Many naphthalene-containing compounds exhibit a wide spectrum of pharmacological activities, such as antiplasmodial, cytotoxic, antibacterial, antiproliferative, antimalarial, and anticancer activity [30, 31]. Herein, we selected a naphthalene-based Schiff base, $H_2\mathbf{L}$ {$H_2\mathbf{L}$ = trans-N,N′-bis-(2-hydroxy-1-naphthalidehydene)-cyclohexanediamine}, and obtained an oxo-bridged dinuclear complex [$Fe_2\mathbf{L}_2(\mu$-O)]. Several similar Fe_2 compounds containing the Fe–O–Fe unit have been synthesized and characterized by magnetic susceptibility measurements [32–35].

Investigation on the effect of chemicals on drug–protein binding is useful to understand the transport and mechanism of the drug in the body. Serum albumin constitutes 55% of the total protein in blood plasma and plays a pivotal role in drug transport and drug metabolism. Recently, the interactions between serum albumin and chemicals have attracted increasing interest [36]. Therefore, we expect the molecular design which combines diferric centers and rigid naphthalene moieties to further enhance DNA cleavage and protein

binding activity. Thus, the synthesis, characterization, magnetism, DNA binding, and cleavage activities of the complex have been described.

2. Experimental setup

2.1. *Materials and instrumentation*

All reagents and chemicals were purchased from commercial sources and used as received. Plasmid pBR322 DNA, agarose, ethidium bromide (EB), bovine serum albumin (BSA), and calf thymus (CT)-DNA were obtained from Sigma. Stock solutions of the complex (5.0×10^{-4} M in 100% DMF) were stored at 4 °C and used for required concentrations of all experiments. Tris–HCl and phosphate buffer solution were prepared using de-ionized, sonicated triple-distilled water. Elemental analyses for C, H, and N were obtained on a Perkin-Elmer analyzer model 240. Infrared spectra were recorded as KBr pellets using a Perkin-Elmer FT-IR spectrometer from 4000 to 400 cm^{-1}. Electronic spectra were measured on a JASCO V-570 spectrophotometer. Fluorescence spectral data were obtained on a MPF-4 fluorescence spectrophotometer at room temperature. Gel imaging and documentation, DigiDoc-It System, were assessed using Labworks Imaging and Analysis Software (UVI, England).

2.2. *Synthesis of the complex*

2.2.1. Synthesis of H_2L. A solution of trans-1,2-diaminocyclohexane (0.46 g, 4 mM) in methanol (10 mL) was added to a stirred solution of 2-hydroxy-1-naphthaldehyde (1.38 g, 8 mM) in methanol (30 mL). The reaction mixture was heated to reflux, stirred for 5 h, and then filtered. A yellow precipitate was obtained (yield: 68%). Elemental analysis (%): Calcd for $C_{28}H_{26}N_2O_2$: C, 79.59; H, 6.20; N, 6.63. Found: C, 78.89; H, 6.34; N, 6.78.

2.2.2. Synthesis of [Fe_2L_2(μ-O)]. A solution of $FeSO_4 \cdot 7H_2O$ (55.6 mg, 0.2 mM) in 10 mL water was added to a solution of H_2L (84.5 mg, 0.2 mM) in 15 mL methanol and refluxed. The reaction mixture was stirred for 2 h. After filtration, a dark red solid was obtained. The crude product was dissolved in DMF. After several days, red block crystals suitable for X-ray diffraction were obtained by slow evaporation, collected by filtration, washed with diethyl ether, and air-dried. Elemental analysis (%): Calcd for $C_{56}H_{48}Fe_2N_4O_5$: C, 69.43; H, 4.99; N, 5.78. Found: C, 70.02; H, 4.67; N, 5.94.

2.3. *X-ray crystallography*

Diffraction data of the complex were collected at 293(2) K with a Bruker Smart 1000 CCD diffractometer using Mo-$K\alpha$ radiation ($\lambda = 0.71073$ Å) with the $\omega-2\theta$ scan technique. The structure was solved by direct methods and refined by full-matrix least-squares method on F^2 using SHELXL-97 [37, 38]. Hydrogens were added theoretically, riding on the concerned atoms, and refined with fixed thermal factors. The details of crystallographic data and structure refinement parameters are summarized in table 1. Selected bond angles and distances are listed in table 2.

Table 1. Crystal data and structure refinement for the complex.

Empirical formula	$C_{56}H_{48}Fe_2N_4O_5$
Formula weight	968.68
Crystal system	Triclinic
Space group	$P-1$
a (Å)	12.658(3)
b (Å)	13.880(3)
c (Å)	14.972(3)
α (°)	116.76(3)
β (°)	105.23(3)
γ (°)	97.75(3)
Volume (Å^3)	2166.3(7)
Z	2
Calculated density (mg m^{-3})	1.485
F (000)	1008
θ Range (°) for data collection	1.67–25.00
Reflections collected/unique	19,738/7462
Data/restraints/parameters	7462/6/662
Goodness of fit on F^2	1.265
R_1, wR_2	$R_1 = 0.0815$, $wR_2 = 0.1691$
Largest diff. peak and hole (e Å^{-3})	0.406 and −0.630

Table 2. Selected bond lengths (Å) and angles (°) for the complex.

Bond distances (Å)			
Fe(1)–O(3)	1.771(4)	Fe(1)–O(1)	1.935(4)
Fe(1)–O(2)	1.952(4)	Fe(1)–N(1)	2.092(5)
Fe(1)–N(2)	2.101(5)	Fe(2)–O(3)	1.795(4)
Fe(2)–O(5)	1.925(4)	Fe(2)–O(4)	1.935(4)
Fe(2)–N(4)	2.094(5)	Fe(2)–N(3)	2.111(5)
Bond angles (°)			
O(3)–Fe(1)–O(1)	111.28(17)	O(3)–Fe(1)–O(2)	106.28(17)
O(1)–Fe(1)–O(2)	91.46(16)	O(3)–Fe(1)–N(1	103.06(19)
O(1)–Fe(1)–N(1)	84.81(17)	O(3)–Fe(1)–N(2)	111.1(2)
O(1)–Fe(1)–N(2)	136.6(2)	O(2)–Fe(1)–N(2)	85.45(18)
N(1)–Fe(1)–N(2)	77.07(18)	O(3)–Fe(2)–O(5)	111.73(17)
O(3)–Fe(2)–O(4)	106.38(17)	O(5)–Fe(2)–O(4)	94.20(16)
O(3)–Fe(2)–N(4)	102.0(2)	O(5)–Fe(2)–N(4)	84.40(19)
O(4)–Fe(2)–N(4)	149.85(19)	O(3)–Fe(2)–N(3)	109.4(2)
O(5)–Fe(2)–N(3)	137.3(2)	O(4)–Fe(2)–N(3)	85.06(17)
N(4)–Fe(2)–N(3)	76.12(19)	O(2)–Fe(1)–N(1)	149.70(19)
Fe(1)–O(3)–Fe(2)	142.9(2)		

2.4. *DNA binding and cleavage experiments*

Solution of CT-DNA gave a ratio of UV absorbance at 260 and 280 nm (A_{260}/A_{280}) of 1.8–1.9, indicating that the DNA was sufficiently free of protein [39]. The stock solution of CT-DNA was prepared in Tris–HCl/NaCl buffer (pH 7.2, stored at 4 °C and used after no more than 4 days). The concentration of CT-DNA was determined from its absorption intensity at 260 nm with a molar extinction coefficient of 6600 M^{-1} cm^{-1} [40]. The absorption spectra of the complex binding to DNA were performed by increasing amounts of CT-DNA to the complex in Tris–HCl buffer (pH 7.2).

The relative bindings of the complex to CT-DNA were studied with an EB-bound CT-DNA solution in 5 mM Tris–HCl/NaCl buffer (pH 7.2) using the fluorescence spectral

method. Fluorescence spectra were recorded at room temperature with excitation at 510 nm and emission at 602 nm. The experiment was carried out by titrating complexes into EB-DNA solution.

DNA cleavage experiments were done by agarose gel electrophoresis on a 20 mL total sample volume in 0.5 mL Eppendorf microcentrifuge tubes, performed by incubation at 37 °C. pBR322DNA (0.1 μg μL^{-1}) in 50 mM Tris–HCl/18 mM NaCl buffer (pH 7.2) was treated with different complex concentrations in the presence of hydrogen peroxide (5 mM). The samples were incubated for 3 h and 2 μL loading buffer was added. Then, the samples were electrophoresed for 2 h at 80 V on 0.8% agarose gel using Tris-boric acid-EDTA buffer (pH 8.2). After electrophoresis, bands were visualized by UV light and photographed.

2.5. *Protein binding studies*

The protein binding study was performed by tryptophan fluorescence quenching experiments using BSA stock solution (1.5 mM) in 10 mM phosphate buffer (pH 7.0). A concentrated stock solution of the compounds was prepared for use in DNA binding experiments, with the exception that phosphate buffer was used instead of a Tris–HCl buffer for all of the experiments. The fluorescence spectra were recorded at room temperature with excitation wavelength of BSA at 280 nm and the emission at 342 nm by keeping the concentration of BSA constant (29.4 μM) while varying the complex concentration from 0 to 12.5 μM.

3. Results and discussion

3.1. *Description of the crystal structure*

The complex has been structurally characterized by single-crystal X-ray crystallography. The structure consists of two iron(III) cations, two $\mathbf{L}^{2-}$ ligands, and a bridged-oxo unit. The drawing of the molecule is shown in figure 1.

$H_2\mathbf{L}$ is composed of three moieties, a cyclohexane and two rigid naphthalene rings. Each diiron(III) complex has two five-coordinate Fe(III) ions that are bridged by an oxo. $H_2\mathbf{L}$ coordinates one iron in a quadridentate mode with N_2O_2 donor sets derived from two diaminocyclohexane-N and two 2-hydroxynaphthaldehyde-O. Both the iron centers are substantially protruded from the ligand planes, which represents the typical five-coordinate square-pyramidal arrangement. Deviations of the metals from the equatorial planes are 0.620 Å (Fe1) and 0.603 Å (Fe2). The fundamental structural component, μ-oxo bridged Fe–O–Fe, commonly occurred with variable bridge angles of 139–180° [41, 42], in accord with the angle 142.851° in [$Fe_2\mathbf{L}_2(\mu$-O)]. The structure shows a 3.38 Å separation of Fe–Fe that falls in the common range of 3.35–3.55 Å. This was attributed to the Fe–Fe distances in the μ-oxo diiron(III) complexes, where Schiff base ligands usually show significantly shorter Fe–Fe distances due to the bent Fe–O–Fe bonds [43–45].

3.2. *IR spectra*

Because of the coupling of several vibrational modes close to each other, it is hard to assign bands of Schiff base species. Therefore, the vibrational spectrum data of a mononuclear Cu

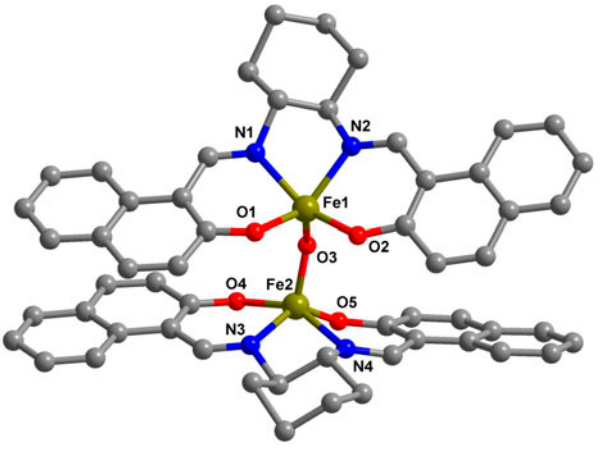

Figure 1. The complex molecule structures and atom-labeling scheme.

(II) complex with a similar ligand was used for comparison [46]. IR band assignments are listed in table 3. The comparison demonstrated comparable vibrational bands between the two complexes due to the analogous ligand. As previously reported, the symmetric stretch and the asymmetric stretch can be quantitatively calculated by the equation [47]: $\lambda_s = [\mu_M + \mu_0(1 + \cos\varphi)](k + k_{MOM})$, $\lambda_{as} = [\mu_M + \mu_0(1 - \cos\varphi)](k - k_{MOM}$, where $\lambda = (5.889 \times 10^{-7})\nu^2$, ν being the frequency (cm^{-1}), k is the M–O stretching force constant and k_{MOM} is the stretch–stretch interaction constant (mdyn $Å^{-1}$), φ is the M–O–M angle (°), and μ_M and μ_0 are the reciprocal masses of the labeled atoms. Due to $k = 3.3$ mdyn $Å^{-1}$ and $k_{MOM} = 0.1$–0.6 mdyn $Å^{-1}$ for the diiron(III) complexes [48] and the Fe–O–Fe angle of 142.851°, the ranges of the ν_s and the ν_{as} were 473.8–419 and 841–772.6 cm^{-1}, respectively. So the band at 456.86 and 824.20 cm^{-1} could be assigned to the symmetric stretch and the asymmetric stretch, respectively.

3.3. *Magnetic properties*

Variable-temperature magnetic susceptibility measurements for the complex were performed on powdered samples for the complex from 2 to 300 K temperature and are shown as plots of χ_M and $\chi_M T$ *versus* T in figure 2. The effective magnetic moment at 300 K is 3.16 B.M. which is lower than the spin-only value (8.36 B.M.) expected for two magnetically diluted high-spin d^5 iron(III) ions. This indicates strong antiferromagnetic interaction in the complex [49]. The values of χ_M decreased slowly with cooling to ca. 50 K with a rapid decrease on the values of $\chi_M T$. On further cooling, the $\chi_M T$ *versus* T plot reaches an approximate plateau, while the χ_M value increases sharply. This low-temperature phenomenon is due to the presence of small quantities (ρ%) of paramagnetic impurities [50]. The magnetic behavior of the compound was interpreted by the use of the Heisenberg–Dirac–van Vleck spin Hamiltonian ($H = -2JS_1S_2$) with $S_1 = S_2 = 5/2$, where S_1 and S_2 are the spin operators for the two iron(III) centers [51]. In this case, the molar magnetic susceptibility data (χ_M) are fit by the expression: $\chi_M = (1 - \rho)(A/B)2Ng^2\beta^2/kT + 4.375\rho/T + \text{t.i.p}$ where $A = 55e^{30J/kT} + 30e^{20J/kT} + 14e^{12J/kT} + 5e^{6J/kT} + e^{2J/kT}$, $B = 11e^{30J/kT} + 9e^{20J/kT} + 7e^{12J/kT} + 5e^{6J/kT} + 3e^{2J/kT} + 1$, J is the exchange coupling parameter between S_1 and S_2, and the other symbols

Table 3. IR assignment of the diiron complex and the copper complex.

Assignment	The diiron complex wave number (cm^{-1})	The copper complex wave number (cm^{-1})
s. ν(Fe–O–Fe)	456.86	–
as. ν(Fe–O) + *as.* ν(Fe–N)	502.23	–
as. ν(Cu–O) + *as.* ν(Cu–N)	–	554.87
s. ω(CH) Ar.	736.03	740.10
as. ν(Fe–O–Fe)	824.20	–
θ(chxn.)	856.30	855.61
as. ω(CH) Ar.	913.71	913.73
as. ω CH(Ar.) + $\delta(CH_2)$	981.69	979.90
ω(CH) imine + θ(naphth.) + *as.* ω(CH) Ar.	1032.42	1037.54
$\nu(C_{methine}–N)$ + θ(naphth.)	1091.86	1091.87
$\delta(CH_2)$ + θ(naphth.)	1138.28	1142.57
γ(CH) Ar. + θ(naphth.) + *as.* ω(CH) Ar.	1181.59	1184.37
γ(CH) Ar.	1209.66	1212.41
γ(CH) Ar. + θ(naphth.) + $\delta(CH_2)$	1245.48	1247.54
as. $\omega(CH_2)$	1304.40	1309.63
as. $\omega(CH_2)$ + β(methyne) + γ(CH) Ar.	1342.32	1343.50
ν(C–O) + α(naphth.) + γ(CH) im.	1395.66	1395.90
γ(CH) Ar. + γ(CH) im. + ν(C=N) + *s.* $\omega(CH_2)$	1430.50	1433.47
γ(CH) Ar. + ν(C=N)	1454.35	1458.49
$\zeta(CH_2)$	1505.98	1506.27
ν(Ar. C=C)	1540.79	1540.62
ν(C=N) + ν(C=C) Ar.	1615.00	1618.21
s. $\nu(CH_2)$	2851.56	2857.61
as. $\nu(CH_2)$	2925.08	2933.72
ν(CH) Ar.	3054.70	3052.08

Note: *v,* stretching; *θ,* ring breathing; *ω,* wagging; *γ,* rocking; *δ,* twisting; *β,* bending; *α,* skeletal; *ζ,* scissoring; *s,* symmetric; *as.,* asymmetric; *naphth.,* naphthalene; *Ar.,* aromatic; *chxn.,* cyclohexane; *im.,* imine.

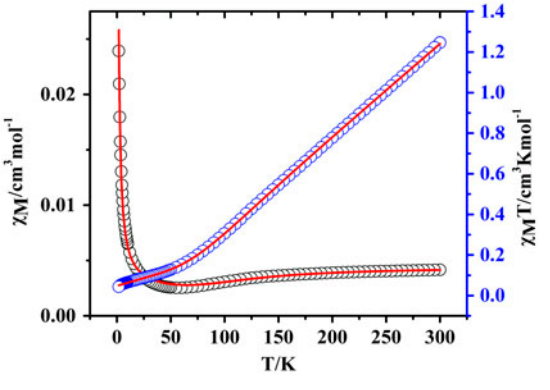

Figure 2. χ_M *vs. T* and $\chi_M T$ *vs. T* plots. Solid lines represent the best theoretical fits.

have their usual meanings. An excellent simulation of the experimental results is obtained with $J = -112\ cm^{-1}$, $g = 1.98$, $\rho = 1.1\%$ ($R = 0.9999$). For unsupported binuclear, structurally characterized, μ-oxo diiron(III) complexes, the magnitude of the coupling is −65 to $-191\ cm^{-1}$ [52]. Gorun and Lippard have also proposed a quantitative relationship between J_{AF} and the shortest super exchange pathway for μ-oxo bridged iron(III) complexes

[53]: $-J = 8.763 \times 10^{11}$ exp($-12.663P$), where the parameter P was defined as half of the shortest superexchange pathway between two metals. The calculated $J = -118\ \mathrm{cm}^{-1}$ for the complex was obtained, which was 5% greater than that of the fitted value.

3.4. *DNA binding properties by UV–vis titration, fluorescence spectroscopic study, and viscosity measurement*

3.4.1. UV–vis titration. Electronic absorption spectroscopy is an effective method to examine the binding mode of DNA with the metal complex. It could be used to determine the equilibrium binding constant (K_b) and the binding site size (s) of the complex to the CT-DNA. Due to a strong stacking interaction between the aromatic chromophore of the ligand and the base pairs of the DNA, the π^* orbital of the intercalated ligand can couple with the π orbital of the base pairs. If the coupling π orbital is partially filled by electrons, it results in decreasing the transition probabilities, which shows hypochromism [54, 55]. The absorption spectral traces of the complex with increasing concentration of CT-DNA are shown in figure 3. With an increase of CT-DNA concentration, the complex showed a significant hypochromism of ~40%, indicating that an intercalation exists between DNA and the complex. The bands in the region 240–260 nm can be attributed to the π–π^* transition of the naphthalene ring of 2-hydroxynaphthaldehyde, and the bands at 300–310 nm are assigned to the π–π^* transition of the azomethine chromophore [56]. For the complex, the band at 370–380 nm can be attributed to the charge transfer (CT) transition [57, 58]. In order to determine the binding strength of the complex with CT-DNA, the equilibrium binding constant K_b and the binding site size s were obtained from a non-linear fitting by the equation [59]: $(\varepsilon_a - \varepsilon_f)/(\varepsilon_b - \varepsilon_f) = (b - (b^2 - 2K_b{}^2C_t[\mathrm{DNA}]_t/s)^{1/2})/2K_bC_t$, $b = 1 + K_bC_t + K_b[\mathrm{DNA}]_t/2s$, where K_b is the microscopic equilibrium binding constant for each site, C_t is the total concentration of the metal complex, s is the site size of the metal complex interacting with the DNA, [DNA] is the concentration of DNA in nucleotides, ε_f, ε_a and ε_b are the molar extinction coefficients of the free complex in solution, the

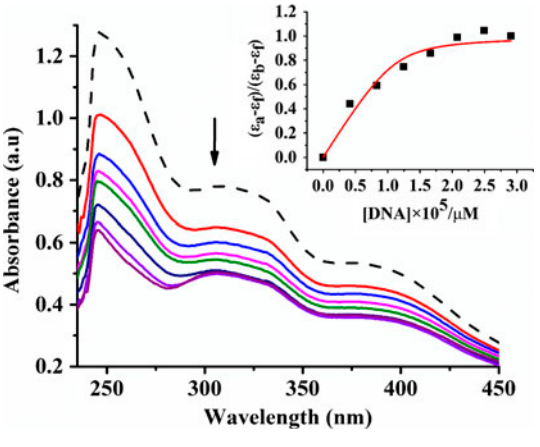

Figure 3. Absorption spectra of complex (5×10^{-4} M) in the absence (dashed line) and presence (solid line) of increasing amounts of CT-DNA in 5 mM Tris–HCl/50 mM NaCl buffer (pH 7.2). The arrow shows the absorbance changes on increasing DNA concentration. Inset: Plots of $(\varepsilon_a - \varepsilon_f)/(\varepsilon_b - \varepsilon_f)$ *vs.* [DNA].

complex bound to DNA at a definite concentration and the complex in completely bound form with CT-DNA, respectively [60]; K_b and s values are $5.9 \times 10^4\ M^{-1}$ and 0.22, respectively. Both of the Schiff base complexes $Fe_2^{III}(\mu\text{-OMe})_2(H_2Hbab)_2$ and $Fe_2^{II}(H_2Hbach)_2(N\text{-MeIm})_2$ [61] are approximately equal to the binding strength obtained by fitting herein ($\sim 10^4$). In addition, the value of K_b is also comparable to previously reported μ-oxo diiron (III) complexes [62–64].

3.4.2. Fluorescence spectroscopic study. The DNA binding nature of the complex has been further discussed by fluorescence spectroscopic study. Emission intensity of EB was used as a spectral probe [65]. Due to no fluorescence emitting for the binuclear complex itself, the interaction between the complex and DNA cannot be studied in a direct method. Since the free EB showed no apparent emission intensity in buffer solution due to the quenching by solvent molecules and the emission intensity being significantly enhanced when EB bound to DNA intercalatively [66], increasing amounts of the diiron(III) complex were added. The competitive binding of the complex to DNA decreased the emission intensity of EB. The fluorescence intensities of EB at 602 (510 nm excitation) with an increasing amount of the complex concentration were recorded. The fluorescence quenching curve of EB bound CT-DNA by the complex is in agreement with the classical linear Stern–Volmer equation [67, 68]: $I_0/I = 1 + K$[complex], where I_0 is the emission intensity of EB-DNA in the absence of complex and I is the emission intensity of EB-DNA in the presence of complex. The linear plot of I_0/I *versus* [complex] gives a measure of the fluorescence intensity changes (figure 4). The K value of the complex was calculated as 3234 ($R = 0.989$). By taking a DNA binding constant of $1.0 \times 10^7\ M^{-1}$ for EB and the complex concentration of the value at a 50% reduction of the fluorescence intensity of EB, an apparent DNA binding constant K_{app} of the complex ($1.6 \times 10^6\ M^{-1}$) was derived from the equation: $K_{EB}[EB] = K_{app}[complex]$, which is less than the binding constant of classical intercalations. This suggests that the complex interacts with DNA through medium binding strength. This is consistent with the above UV–vis observations. As previous work shows, the apparent DNA binding constant K_{app} of salen Schiff base complexes (Salen = salicylaldehydoethylenediamine [69]) falls in the range

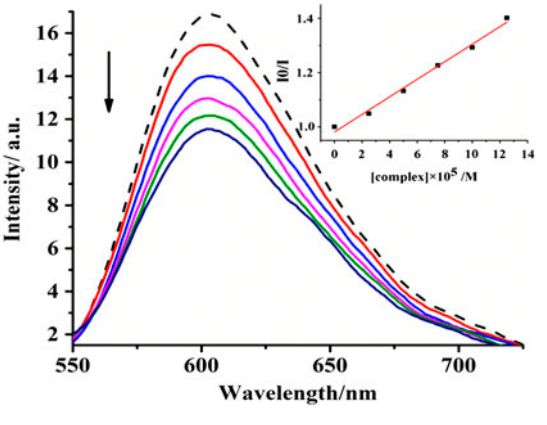

Figure 4. Fluorescence emission spectra of EB-DNA system in the absence (dashed line) and presence (solid lines) of increasing amounts of complex (5×10^{-4} M). The arrow shows the intensity changes on increasing complex concentration. Inset: the plot of I_0/I *vs.* the complex concentration.

1×10^5 to $5 \times 10^5\ M^{-1}$, such as [FeSalen]Cl ($5 \times 10^5\ M^{-1}$) [70], Et_2Sn(Salen) ($1 \times 10^5\ M^{-1}$) [71], bis-sodium(5sulfosalicylaldehyde)-o-phenylendiiminato) manganese(III) acetate ($3.6 \times 10^5\ M^{-1}$) [72], etc. Compared with the examples, the complex we have synthesized can strongly interact with DNA and is efficiently protected by DNA. The greater K_{app} may be due to the presence of a more aromatic moiety, which enhances the binding propensity of the molecule to DNA.

3.4.3. Viscosity measurement. As a means for further clarifying the binding mode of the binuclear complex with DNA, viscosity measurements were carried out on calf thymus (CT)-DNA by varying the concentration of the complex. When the complex interacts with DNA in a classical intercalation model, DNA base pairs would be separated to accommodate the complex, resulting in an increase in overall DNA length; hence, the viscosity of the DNA solution increased [73]. The plot of $(\eta/\eta_0)^{1/3}$ *versus* [complex]/[DNA] gives a measure of the viscosity changes (figure 5). As the figure demonstrated, the viscosity of DNA increases steadily with increasing concentration of the complex. This suggests that due to the presence of the naphthalene ring in both parts of the ligand, the complex binds to DNA through a classical intercalation mode, which is analogous to complex **1** mentioned previously [74].

3.5. *DNA cleavage study*

The DNA cleavage activity of the complex was investigated by agarose gel electrophoresis. We studied the interaction of the complex with pBR322 DNA by monitoring the conversion of circular super coiled DNA (Form I) to nicked DNA (Form II) via concentration-dependent experiments. The results of the gel electrophoresis separation of plasmid pBR322 DNA treated with the complex only and in the presence of H_2O_2 are depicted in figure 6(a) and (b), respectively. A comparison between two control experiments indicated the DNA cleavage efficiencies exhibit remarkable increases in the presence of H_2O_2. Control experiments also suggest that untreated DNA and DNA incubated with the peroxide alone did not show any

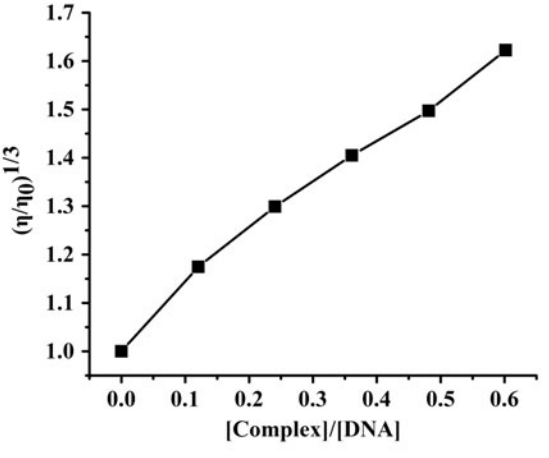

Figure 5. The plot of $(\eta/\eta_0)^{1/3}$ *vs*. [complex]/ [DNA] at 25 °C.

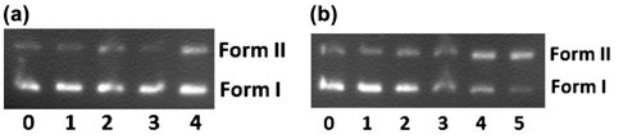

Figure 6. (a) Agarose gel electrophoresis of pBR322 plasmid DNA treated with complex at different concentrations. Lane 0: supercoiled DNA (control); Lanes 1–4: complex (5, 20, 35, 50 μM). (b) Agarose gel electrophoresis of pBR322 plasmid DNA treated with complex at different concentrations with addition of hydrogen peroxide. Lane 0: supercoiled DNA (control); Lane 1: H_2O_2 (5 μM); Lanes 2–5: 5 μM H_2O_2 + complex (5, 20, 35, 50 μM).

significant DNA cleavage. As the figures show, the proportion of the supercoiled (Form I) DNA which was cleaved to Form II in the concentration (50 μM) of the complex and the presence of H_2O_2 [Lane 5 in figure 6(b)] is notably higher than those incubated with the complex alone [Lane 4 in figure 6(a)]. As Chowdhury *et al.* have mentioned [75], this implies that H_2O_2 is a revulsive or an activator that plays a vital role [76].

3.6. *Protein binding study*

Interactions between serum albumin and chemicals have attracted many researchers because serum albumin is contained in more than 55% of the total protein in blood plasma and plays a pivotal role in drug transport and drug metabolism. Serum albumin is also well known to bind small aromatics [77]. BSA is the most extensively studied serum albumin due to its structural homology with human serum albumin. The interaction of BSA with the complex was investigated by tryptophan residues emission-quenching experiments at room temperature. The fluorescence spectra were recorded from 290 to 450 nm upon excitation at 280 nm. Since serum albumin molecules are well known to bind small aromatics, the intensity of the characteristic broad emission band at 345 nm decreased gradually with increasing amounts of the complex (shown in figure 7). The observed quenching may be attributed to changes in the secondary structure of BSA in phosphate buffer medium that may affect the

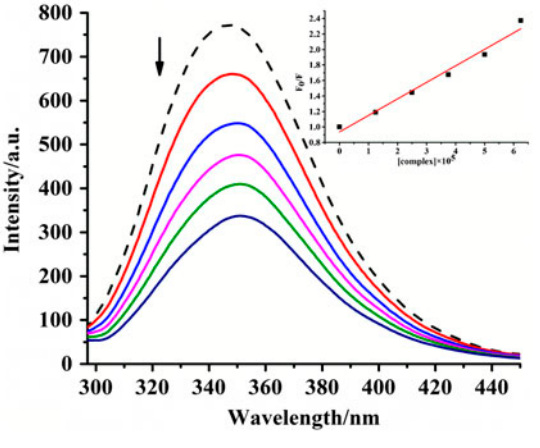

Figure 7. Fluorescence emission spectra of the BSA system in the absence (dashed line) and presence (solid lines) of increasing amounts of complex (5×10^{-4} M). Inset: the plot of F_0/F *vs*. the complex concentration.

orientation of the tryptophan residues of BSA, thus indicating an interaction between BSA and the complex. The fluorescence quenching is quantitatively calculated by the Stern–Volmer equation, $F_0/F = 1 + K_q\tau_0[Q] = 1 + K_{sv}[Q]$, where F_0 and F represent the fluorescence intensities in the absence and in the presence of quencher, K_q is the quenching rate constant, τ_0 the average lifetime of the biomolecule without quencher (about 10^{-8} s) [67], K_{SV} the Stern–Volmer quenching constant, and [Q] the concentration of quencher. Then the calculated value of K_{sv} and K_q are $2.13 \times 10^4\,M^{-1}$ and $2.13 \times 10^{12}\,M^{-1}s^{-1}$, respectively.

The quenching mechanisms could be classified as dynamic quenching or static quenching. Dynamic quenching refers to a process in which the fluorophore and the quencher come into contact during the transient existence of the exited state. Static quenching refers to fluorophore–quencher complex formation. The maximum scatter collision-quenching constant of diverse kinds of quenchers for biopolymer fluorescence would usually be $2.0 \times 10^{10}\,M^{-1}s^{-1}$, which is lower than the K_q value ($2.13 \times 10^{12}\,M^{-1}s^{-1}$), implying the existence of static quenching [78].

For the static quenching interaction, the binding constant (K) and the number of binding sites (n) can be confirmed according to the Scatchard equation: $\log(F_0 - F)/F = \log K + n\log[Q]$. In the linear fit plot of $\log(F_0 - F)/F$ *versus* $\log[Q]$, the slope and the intercept could be used to calculate K and n, which gave us the values as $1.36 \times 10^5\,M^{-1}$ and 1.20, respectively. The value of n was approximately equal to 1, which indicated that there was just one binding site in BSA for the complex. Then the complex was contrasted with another diiron complex $Fe_2(\mu\text{-}O)(\mathbf{L}\text{-his})_2(B)_2](ClO_4)_2$, which has been demonstrated before [62]. According to the literature, the latter had a lower binding constant K ($3.6 \times 10^4\,M^{-1}$), which might be attributed to its poor planarity compared to the complex we synthesized. The binding constant value of $10^5\,M^{-1}$ suggest moderate binding propensity of the complex to BSA [79].

4. Conclusion

We have synthesized a new oxo-bridged iron complex and investigated its chemical nuclease activity and variable-temperature magnetic susceptibility. The effective magnetic moment at 300 K (3.16 B.M.) demonstrated a strong antiferromagnetic interaction between two magnetically diluted high-spin d^5 iron(III) ions. Due to the presence of the aromatic moiety (naphthalene ring) in the Schiff base ligand, UV–vis titration indicated that intercalation exists between DNA and the complex, and the binding constant of the complex with CT-DNA is $K_{app} = 1.6 \times 10^6\,M^{-1}$, indicating that the complex interacts with DNA through a medium binding strength. Furthermore, the fluorescence spectroscopic study and viscosity measurement are in accord with the above conclusion.

Supplementary material

Crystallographic data (excluding structure factors) for the structures in this article have been deposited with the Cambridge Crystallographic Data Center as supplementary publication CCDC 977272. Copies of the data can be obtained, free of charge, on application to the CCDC, 12 Union Road, Cambridge CB2 1EZ, UK.

Funding

This work was supported by the National Natural Science Foundation of China [grant number 21171101] and [grant number 21001066]; Tianjin Science Foundation [grant number 12JCYBJC13600]; MOE Innovation Team [grant number IRT13022] of China and NFFTBS [grant number J1103306].

References

[1] E. Nakata, T. Nakanishi, A. Kawai, K. Asaumi, T. Yamaai, M. Asano, T. Nishida, S. Mitani, H. Inoue, M. Takigawa. *Bone*, **31**, 441 (2002).
[2] E. Falcieri, P. Gobbi, P. Sabatelli, S. Santi, F. Farabegoli, R. Rana, A. Cataldi, N.M. Maraldi, A.M. Martelli. *Histochemistry*, **98**, 121 (1992).
[3] Q. Jiang, N. Xiao, P.F. Shi, Y.G. Zhu, Z.J. Guo. *Coord. Chem. Rev.*, **251**, 1951 (2007).
[4] F. Mancin, P. Scrimin, P. Tecillab, U. Tonellato. *Chem. Commun.*, 2540, (2005).
[5] J. Suh. *Acc. Chem. Res.*, **36**, 562 (2003).
[6] J.A. Cowan. *Chem. Rev.*, **98**, 1067 (1998).
[7] N.H. Williams, B. Takasaki, M. Wall. *Acc. Chem. Res.*, **32**, 485 (1999).
[8] E.L. Hegg, J.N. Burstyn. *Coord. Chem. Rev.*, **173**, 133 (1998).
[9] B. Lippert. *BioMetals*, **13**, 195 (1992).
[10] R.B. Weiss, M.C. Christian. *Drugs*, **46**, 360 (1993).
[11] H. Katada, M. Komiyama. *Chem. Biochem.*, **10**, 1279 (2009).
[12] T. Todorovic, U. Rychlewska, B. Warżajtis, D. Radanović, N. Filipović, I. Pajić, D. Sladić, K. Anđelković. *Polyhedron*, **28**, 2397 (2009).
[13] B.D. Wang, Z.Y. Yang, Q. Wang, T.K. Cai, P. Crewdson. *Bioorg. Med. Chem.*, **14**, 1880 (2006).
[14] Y.Y. Karabach, A.M. Kirillov, M. Haukka, M.N. Kopylovich, A.J.L. Pombeiro. *J. Inorg. Biochem.*, **102**, 1190 (2008).
[15] U. Schuchardt, W.A. Carvalho, E.V. Spinacé. *Syntlett*, **10**, 713 (1993).
[16] S. Rekha, K.R. Nagasundara. *Indian J. Chem.*, **A45**, 2421 (2006).
[17] T.P. Yoon, E.N. Jacobsen. *Science*, **299**, 1691 (2003).
[18] C. Shiju, D. Arish, S. Kumaresan. *Spectrochimica*, **105**, 532 (2013).
[19] Y.C. Liu, Z.Y. Yang. *J. Organomet. Chem.*, **694**, 3091 (2009).
[20] Y.C. Liu, Z.Y. Yang. *J. Inorg. Biochem.*, **103**, 1014 (2009).
[21] A. Kulkarni, S.A. Patil, P.S. Badami. *Eur. J. Med. Chem.*, **44**, 2904 (2009).
[22] Y.C. Liu, Z.Y. Yang. *Eur. J. Med. Chem.*, **44**, 5080 (2009).
[23] Y.C. Liu, Z.Y. Yang. *Biometals*, **22**, 733 (2009).
[24] R. Vijayalakshmi, M. Kanthimathi, V. Subramanian, B.U. Nair. *Biochim. Biophys. Acta*, **1475**, 157 (2000).
[25] A.A. El-Sherif, T.M.A. Eldebss. *Spectrochimica*, **79**, 1803 (2011).
[26] I.G. Denisov, T.M. Makris, S.G. Sliga. *Chem. Rev.*, **105**, 2253 (2005).
[27] M. Costas, M.P. Mehn, M.P. Jensen. *Chem. Rev.*, **104**, 939 (2004).
[28] M. Franchini, D. Veneri. *J. Hematol.*, **5**, 287 (2004).
[29] C.P. Siegers, D. Bumann, G. Baretton. *Toxicol. in Vitro*, **5**, 427 (1991).
[30] A.D. Tinoco, E.V. Eames, C.D. Incarvito, A.M. Valentine. *Inorg. Chem.*, **47**, 8380 (2008).
[31] B. Ojha, G. Das. *J. Phys. Chem.*, **114**, 3979 (2010).
[32] J.W. Shin, S.R. Rowthu, J.E. Lee, H.I. Lee, K.S. Min. *Polyhedron*, **33**, 25 (2012).
[33] A.R. Oki, A. Tandilashvili, D. Patel, M. Macillo, E. Wolfe. *J. Coord. Chem.*, **52**, 4 (2001).
[34] J.M. Becker, J. Barker, G.J. Clarkson, R. van Gorkum, G. Johal, R.I. Walton, P. Scott. *Dalton Trans.*, 2309 (2010).
[35] R. Shakya, D.R. Powell, R.P. Houser. *Eur. J. Inorg. Chem.*, **35**, 5319 (2009).
[36] X.L. Wang, M. Jiang, Y.T. Li, Z.Y. Wu, C.W. Yan. *J. Coord. Chem.*, **66**, 1985 (2013).
[37] G.M. Sheldrick. *SHELXS-97, Program for the Solution of Crystal Structure*, University of Göttingen, Germany (1997).
[38] G.M. Sheldrick. *SHELXL-97, Program for the Refinement of Crystal Structure*, University of Göttingen, Germany (1997).
[39] J. Marmur. *J. Mol. Biol.*, **3**, 208 (1961).
[40] Y. Gultneh, A.R. Khan, D. Blaise, S. Chaudhry, B. Ahvazi, B.B. Marvey, R.J. Butcher. *J. Inorg. Biochem.*, **75**, 7 (1999).
[41] R.N. Mukherjee, T.D.P. Stack, R.H. Holm. *J. Am. Chem. Soc.*, **110**, 1850 (1988).
[42] K.S. Murray. *Coord. Chem. Rev.*, **12**, 1 (1974).
[43] K. Oyaizu, E.L. Dewi, E. Tsuchida. *Inorg. Chim. Acta*, **321**, 205 (2001).
[44] M. Gerloch, E.D. McKenzie, A.D.C. Towl. *J. Chem. Soc. (A)*, 2850 (1969).

[45] P. Coggon, A.T. McPhail, F.E. Mabbs, V.N. McLachlan. *J. Chem. Soc. (A)*, 1014 (1971).
[46] H. Karabıyık, O. Erdem, M. Aygun, B. Güzel, S. García-Granda. *J. Inorg. Organomet. Poly. Mater.*, **20**, 142 (2010).
[47] J. Sanders-Loehr, W.D. Wheeler, A.K. Shiemke, B.A. Averill, T.M. Loehr. *J. Am. Chem. Soc.*, **111**, 8084 (1989).
[48] D.M. Kurtz Jr. *Chem. Rev.*, **90**, 585 (1990).
[49] E.J. Seddon, J. Yoo, K. Folting, J.C. Huffman, D.N. Hendrickson, G. Christou. *J. Chem. Soc., Dalton Trans.*, 3640 (2000).
[50] A.R. Li, H.H. Wei, L.L. Gang. *Inorg. Chim. Acta*, **290**, 51 (1999).
[51] S.J. Lippard, C.J. O'Connor. *Prog. Inorg. Chem.*, **29**, 203 (1982).
[52] R.M. Buchanan, R.J. O'Brien, J.F. Richardson, J.M. Latour. *Inorg. Chim. Acta*, **214**, 33 (1993).
[53] S.M. Gorun, S.J. Lippard. *Inorg. Chem.*, **30**, 1625 (1991).
[54] V.A. Bloomfield, D.M. Crothers, I. Tinocco Jr. *Phys. Chem. Nuc. Acids*, 432 (1974).
[55] S. Anbu, M. Kandaswamy, B. Varghese. *Dalton Trans.*, 3823 (2010).
[56] W.J. Ruan, G.H. Hu, S.J. Wang, J.H. Tian, Q.L. Wang, Z.A. Zhu. *Chin. J. Chem.*, **23**, 709 (2005).
[57] R.C. Felicio, E.T.G. Cavalheiro, E.R. Dockal. *Polyhedron*, **20**, 261 (2001).
[58] T. Matsushita, H. Kono, M. Nishino, T. Shono. *Bull. Chem. Soc. Jpn.*, **55**, 2581 (1982).
[59] R.B. Nair, E.S. Teng, S.L. Kirkland, C.J. Murphy. *Inorg. Chem.*, **37**, 139 (1998).
[60] A.M. Pyle, J.P. Rehmann, R. Meshoyrer, C.V. Kumar, N.J. Turro, J.K. Barton. *J. Am. Chem. Soc.*, **111**, 3051 (1989).
[61] P.J. Cappillino, P.C. Tarves, G.T. Rowe, A.J. Lewis, M. Harvey, C. Rogge, A. Stassinopoulos, W. Lo, W.H. Armstrong, J.P. Caradonna. *Inorg. Chim. Acta*, **362**, 2136 (2009).
[62] M. Roy, T. Bhowmick, R. Santhanagopal, S. Ramakumar, A.R. Chakravarty. *Dalton Trans.*, 4671 (2009).
[63] M. Roy, R. Santhanagopal, A.R. Chakravarty. *Dalton Trans.*, 1024 (2009).
[64] X.Q. Chen, X.J. Peng, J.Y. Wang, Y. Wang, S. Wu, L.Z. Zhang, T. Wu, Y.K.Wu. Eur. *J. Inorg. Chem.*, 5400 (2007).
[65] E. Nyarko, N. Hanada, A. Habib, M. Tabata. *Inorg. Chim. Acta*, **357**, 739 (2004).
[66] J.B. Lepecq, C. Paoletti. *J. Mol. Biol.*, **27**, 87 (1967).
[67] J.R. Lakowicz, G. Weber. *Biochemistry*, **12**, 4161 (1973).
[68] G. Pratviel, J. Bernadou, B. Meunier. *Angew. Chem. Int. Ed. Eng.*, **34**, 746 (1995).
[69] P.G. Cozzi. *Chem. Soc. Rev.*, **33**, 410 (2004).
[70] M.N. Dehkordi, P. Lincoln. *J. Fluoresc.*, **23**, 813 (2013).
[71] G.D. Liu, J.P. Liao, Y.Z. Fang, S.S. Huang, G.L. Sheng, R.Q. Yu. *Anal. Sci.*, **18**, 391 (2002).
[72] M.N. Dehkordi, A.K. Bordbar, M.A. Mehrgardi, V. Mirkhani. *J. Fluoresc.*, **21**, 1649 (2011).
[73] J.B. Chaires, N. Dattagupta, D.M. Crothers. *Biochemistry*, **21**, 3933 (1982).
[74] F. Javed, A.A. Altaf, A. Badshah, M.N. Tahir, M. Siddiq, A. Shah, S. Ullah, B. Lal. *J. Coord. Chem.*, **65**, 969 (2012).
[75] S.R. Chowdhury, M.D. Selim, S. Chatterjee, S. Igarashi, Y. Yukawa, K.K. Mukherjea. *J. Coord. Chem.*, **65**, 3469 (2012).
[76] L.M.T. Schnaith, R.S. Hansont, L. Que. *Proc. Natl. Acad. Sci.*, **91**, 569 (1994).
[77] P. Kalaivani, R. Prabhakaran, M.V. Kaveri, R. Huang, R.J. Staples, K. Natarajan. *Inorg. Chim. Acta*, **405**, 415 (2013).
[78] W.R. Ware. *J. Phys. Chem.*, **66**, 455 (1962).
[79] A. Begum, S. Saha, M. Nethaji, A.R. Chakravarty. *Indian J. Chem.*, **48A**, 473 (2009).